Growth of single-walled carbon nanotubes by alcohol chemical vapor deposition with water vapor addition: Narrowing the diameter and chiral angle distributions

Hiroki Takezaki [a], Taiki Inoue [a], Rong Xiang [a], Shohei Chiashi [a], and Shigeo Maruyama [a,b,*]

[a] Department of Mechanical Engineering, The University of Tokyo, 7-3-1 Hongo, Bunkyo-ku, Tokyo 113-8656, Japan

[b] Energy NanoEngineering Laboratory, National Institute of Advanced Industrial Science and Technology (AIST), 1-2-1 Namiki, Tsukuba 305-8564, Japan

[*] Corresponding author.

E-mail address: maruyama@photon.t.u-tokyo.ac.jp (S. Maruyama).

Abstract

We report the structure-controlled growth of single-walled carbon nanotubes (SWCNTs) based on alcohol chemical vapor deposition with the addition of water vapor. The introduction of water vapor during the growth and pretreatment by water vapor were both systematically examined for the growth of SWCNTs. Raman spectroscopy analysis revealed that the addition of water vapor in both cases induced a decrease in the tube diameters, which indicates the importance of catalyst conditioning for the changes in chirality distribution. The selective growth of SWCNTs having small diameters and large chiral angles was achieved by water vapor pretreatment.

1. Introduction

Single-walled carbon nanotubes (SWCNTs) [1] exhibit several extraordinary properties and potential applications in various fields including composites, energy storage, and electronics [2]. Because the metallicity and the bandgaps of SWCNTs are determined by their atomic structure [3], i.e., chirality, their post-growth separation [4] and structure-controlled growth [5–7] have been extensively studied, especially for their applications in electronic [8,9] and optical [10] devices. Because the post-growth separation techniques usually suffer from defect formation in SWCNTs during the dispersion process, direct growth of chirality-controlled SWCNTs is preferable. The chirality of SWCNTs can be identified using a pair of integers (n,m), which can be converted to (d,θ), where d and θ denote the tube diameter and the chiral angle, respectively, using the following equations: $d = \sqrt{3}a_{\mathrm{c-c}}\sqrt{n^2 + m^2 + nm}/\pi$ and $\theta = \tan^{-1}\sqrt{3}\,m/(2n + m)$, where $a_{\mathrm{c\text{-}c}}$ denotes the carbon–carbon bond length. To ensure the chirality-selective growth of SWCNTs with high purity, both the diameter and the chiral angle have to be precisely controlled.

During the growth of SWCNTs via the chemical vapor deposition (CVD) method [11], the carbon source molecules react on the catalyst nanoparticles at a high temperature to form initial cap structures [12], which define the chirality of SWCNTs, and the sidewalls of SWCNTs are grown from the carbon caps [13]. Chirality can change during tube elongation [14]; however, such changes usually occur with low probability [15], except for the intentionally oscillated growth conditions [16,17]. Thus, the chirality of SWCNTs can be effectively controlled by controlling the catalyst structure at the initial nucleation stage. Some specific chiralities are selectively grown using certain lattices of the elaborate alloy catalyst [5]. Further, the diameters of SWCNTs have been controlled in previous studies by controlling the diameter of the catalyst using discrete particles [18], a bimetallic system [19], and at a low growth temperature [20]. In contrast, controlling the chiral angle is more challenging. Even though the chiral angles of as-grown samples usually follow a uniform distribution, the preferential growth of certain chiral angles [21], especially large chiral angles close to 30° [22–26], has been observed in several growth systems. Experimental and theoretical efforts based on both kinetics [27–29] and thermodynamics [29,30] have been devoted to explain the origin of the selectivity.

For the CVD growth of SWCNTs, apart from the major contribution of the catalyst and carbon source species, the addition of other gases to the growth atmosphere can cause various changes in the structures of the produced SWCNTs. For example, sulfur as an additive [31] and NH_3 as a pretreatment gas [25] have been used for the structure-controlled CVD growth of SWCNTs. Furthermore, various studies have shown the effects of water vapor (H_2O) on the SWCNT growth usually as an enhancer to increase the yield [32]. Meanwhile, semiconducting SWCNTs were preferentially grown by controlling the water vapor concentration during the CVD process [33]. As a pretreatment agent for the catalyst, water vapor has been shown to induce the selective synthesis of metallic [34], semiconducting [35], small-diameter [36,37], and specific-chirality [38,39] SWCNTs.

Water vapor plays various roles in the SWCNT growth; however, its effects have not been explored either by focusing on changes in chirality distribution in a wide range or throughout the different CVD stages including catalyst pretreatment and nanotube growth.

In this study, we investigated the effects of the addition of water vapor on the alcohol CVD growth of SWCNTs [20]. We compared SWCNTs obtained without water vapor, with water vapor addition during growth, and with water vapor pretreatment and observed the decrease in the tube diameters. We revealed that water vapor pretreatment significantly affected the changes in chirality distribution. The selective growth of SWCNTs with small diameters and large chiral angles was achieved by water vapor pretreatment.

2. Experimental methods

2.2 Growth of SWCNTs by alcohol CVD with water vapor addition

Co/Mo bimetallic nanoparticles were deposited on Si with 100-nm thick SiO_2 substrates by dip-coating [40] and used as the catalyst for the SWCNT growth. SWCNTs were grown by the low-pressure alcohol CVD method [20] using ethanol as the carbon source gas. After the substrate with catalyst was loaded in the quartz tube and evacuated by a scroll pump, 300 sccm of Ar with 3% H_2 was introduced at 40 kPa. The furnace temperature was increased up to growth temperatures from 650°C to 900°C with flowing Ar/H_2 for 30 min and was maintained for 10 min to reduce the metal nanoparticles. Subsequently, the flow of Ar/H_2 was stopped, and ethanol vapor was introduced at 1300 Pa to grow SWCNTs. To introduce water vapor, a tank filled with distilled water was connected to the CVD setup and was heated at ~80°C using a water bath to increase the vapor pressure. The flow rate of the water vapor was controlled using a mass flow controller, and the total pressure of water vapor and other gases was monitored using a capacitance manometer. Further, we introduced water vapor either during growth along with ethanol or before growth for the pretreatment of the catalyst. The growth time was set to 5 min for all the conditions. The temperature profiles and the gas composition during the CVD processes are summarized in Figure S1.

2.2 Characterization of SWCNTs

The SWCNTs were characterized using scanning electron microscopy (SEM) (Hitachi, S-4800), Raman spectroscopy (Renishaw, inVia), optical absorption spectroscopy (Shimadzu, UV-3150), and photoluminescence (PL) spectroscopy (home-made system based on a detector, Horiba Jobin Yvon, Symphony IGA-1700 and a spectrometer, iHR320). The acceleration voltage for SEM observation was 1 kV. Four excitation lasers with wavelengths of 488, 532, 633, and 785 nm (corresponding to 2.54, 2.33, 1.96, and 1.58 eV, respectively) were used for the Raman measurements.

3. Results and discussions

3.1. Effects of water vapor addition during growth of SWCNTs

SWCNTs were grown from ethanol at 800°C without water (0 Pa, Figure S1a) and with water vapor during growth at different pressures ranging from 30 to 1500 Pa (Figure S1b). The SEM images and Raman spectra of the SWCNTs are denoted in Figure 1. The SEM image indicates that highly-bundled networks of SWCNTs are grown for the sample without water vapor (Figure 1a). However, the growth yield of SWCNTs decreases with increasing water vapor pressure, and SWCNTs lying on the substrates are observed for the sample of water vapor at 1500 Pa (Figure 1c). In the low-frequency region (100–300 cm¯1) of the Raman spectra, the radial breathing mode (RBM) peaks, whose peak frequencies are inversely proportional to the diameters of SWCNTs [41], are observed. As the water pressure increases, the intensities of the RBM peaks with low frequencies decrease, whereas those of the RBM peaks with high frequencies increase for all the four excitation wavelengths (Figure 1d–g). When the partial pressure of the water vapor is higher than 600 Pa, the RBM peaks higher than ~180 cm^{-1}, corresponding to a diameter of less than 1.2 nm, dominate, indicating that the small-diameter SWCNTs are preferentially grown. In the high-frequency region, G-band peaks with a split shape appear at ~1592 cm^{-1}. The large frequency difference between the G^+ and G^- peaks [42] also reveals that the tube diameters decrease with increasing water vapor pressures. The D-band observed at around 1350 cm^{-1} is known to represent the defect concentration of graphitic materials [43]. Even in the case of water vapor at 1500 Pa, no apparent increases are observed in the D-band, which indicates that the obtained SWCNTs are not damaged during growth by water vapor in this conditions.

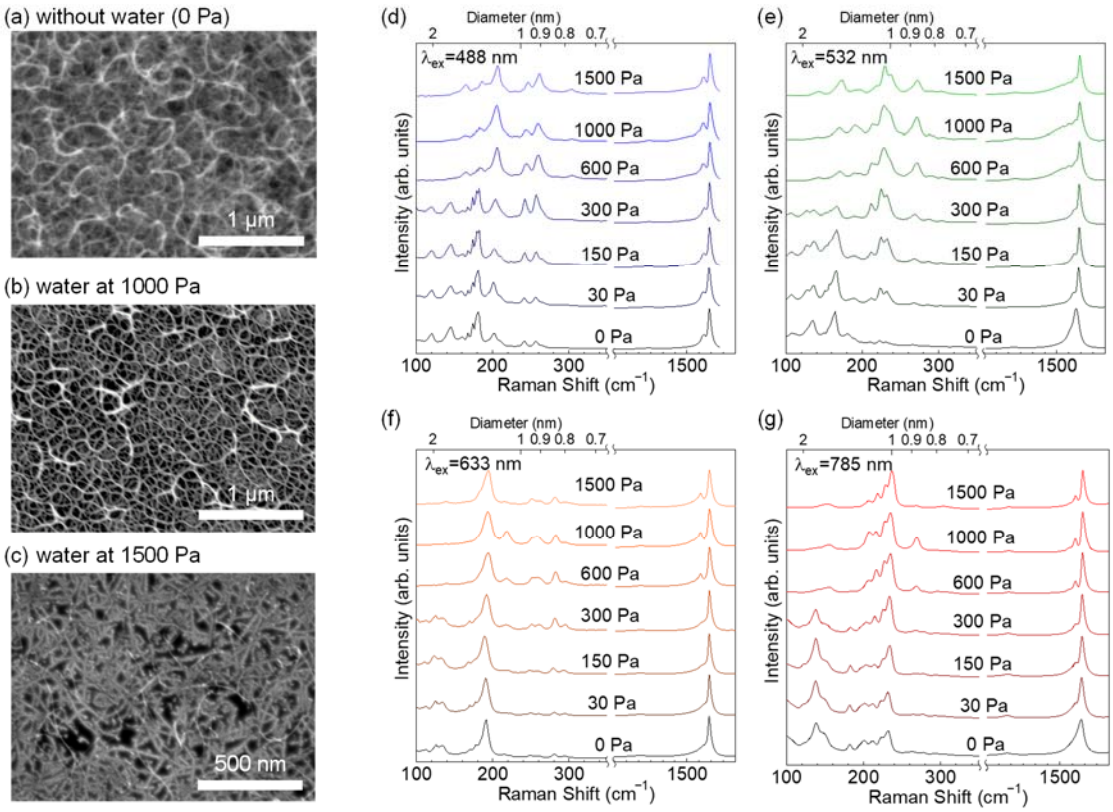

Figure 1. SEM images of SWCNTs grown at 800°C from ethanol: (a) without water (0 Pa); (b) with water vapor at 1000 Pa; and (c) with water vapor at 1500 Pa during growth. Raman spectra of SWCNTs grown with different partial pressures of water vapor measured with excitation wavelengths of (d) 488 nm, (e) 532 nm, (f) 633 nm, and (g) 785 nm.

3.2. Effects of water vapor pretreatment and comparison with water vapor addition during growth

The result that the water vapor addition causes the decrease in nanotube diameters is considered to be related to the catalyst formation process and/or the growth process. To elucidate the origin of the water vapor effect, SWCNTs were grown with water vapor pretreatment, where water vapor was introduced for 5 min before the growth process, and only ethanol was introduced during the growth process (Figure S1c). Figure 2 depicts the RBM Raman spectra of SWCNTs grown under the following three conditions: without water vapor, with water vapor before growth, and with water vapor during growth. When compared with SWCNTs grown without water vapor, SWCNTs grown with water vapor before growth show RBMs of similarly small diameters as those of SWCNTs grown with water vapor during growth.

In addition to the Raman spectra, we also characterized the tube diameters using the optical absorption spectra (Figure S2). The spectra were directly measured on SWCNTs grown on quartz substrates. While the E^{S}_{11} peak of the SWCNTs appears at ~2400 nm for the samples grown without water vapor, the peak can be observed at ~1200 nm for the samples grown with water vapor before

growth, indicating that the average diameter of the SWCNTs are decreased from ~2.0 nm to ~1.0 nm by the water vapor addition before growth. This result agrees well with that obtained from the Raman analysis.

The addition of water vapor before growth alone induced drastic changes in the diameter distribution of SWCNTs, which implies that water mainly affects the catalyst formation process instead of the nanotube growth process. In the case of water vapor addition during growth, water seems to affect the catalyst conditioning at the onset of the growth process and not to lead significant changes in SWCNT structures during the tube elongation stage. Hereafter, we focus on the effect of water vapor before growth (water vapor pretreatment).

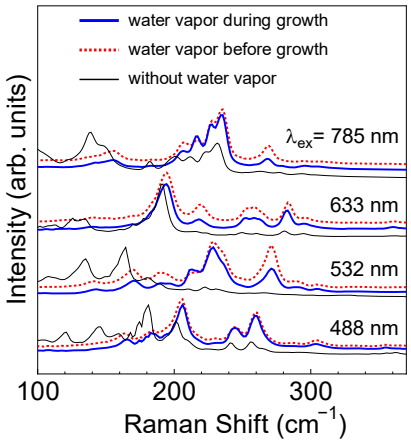

Figure 2. Raman spectra of SWCNTs grown at 800°C without water vapor, with water vapor during growth at 600 Pa, and with water vapor before growth at 600 Pa.

3.3. Effects of water pretreatment temperature and growth temperature

We investigated the pretreatment temperature and the growth temperature as two independent factors. As the first factor, the pretreatment temperature of water vapor was varied to 900°C, 800°C, and 700°C while maintaining the growth temperature at 800°C (Figure S3). All the growth conditions yielded SWCNTs; however, the growth amount of SWCNTs was small at 900°C. From the RBMs, the diameters of SWCNTs obtained with pretreatment at 900°C are larger than those at 800°C and 700°C. This is because a high temperature causes the aggregation of the catalyst nanoparticles and results in the growth of SWCNTs with large diameters. No significant difference can be observed between the RBM peaks at pretreatment temperatures of 800°C and 700°C. In the following experiments, the water pretreatment temperature was set to 800°C.

As the second factor, we changed the growth temperature while keeping the pretreatment temperature. The growth temperature was varied to 800°C, 700°C, and 650°C after water vapor pretreatment was conducted at 800°C and 600 Pa. The Raman spectra in the high-frequency range and

the SEM images of the samples are depicted in Figure S4. The relative intensity of the D-band is observed to increase with decreasing growth temperature. The yield of SWCNTs also decreases at low temperature. The RBM Raman spectra of the samples are denoted in Figure 3 along with the empirical Kataura plot [44]. For the SWCNTs grown at 650°C and 700°C, the RBM peaks below 200 cm^{-1} are highly suppressed, while those at 200–250 cm^{-1} become prominent. These observed changes in the RBM Raman spectra indicate that the low growth temperature leads to the growth of small-diameter SWCNTs with a narrow distribution, similar to that found in previous studies [23,45]. In addition to the changes in diameter distribution, there are some distinctively weakened RBM peaks in the spectra ranging from 200 to 250 cm^{-1} when the growth temperature decreases from 800°C to 700°C and 650°C. These include the 206-cm^{-1} peak at 488-nm excitation, the 270-cm^{-1} peak at 532-nm excitation, the 219-cm^{-1} peak at 633-nm excitation, and the 269-cm^{-1} peak at 785-nm excitation, which can be assigned to (14,1), (9,3), (13,1), and (11,0), respectively. The procedures of chirality assignment are described in a later section. Here, the decreased chiralities are near-zigzag SWCNTs possessing a chiral angle that is close to 0°. These changes cannot be solely explained by the changes in diameter distribution; hence, the details of the chirality distribution have to be examined.

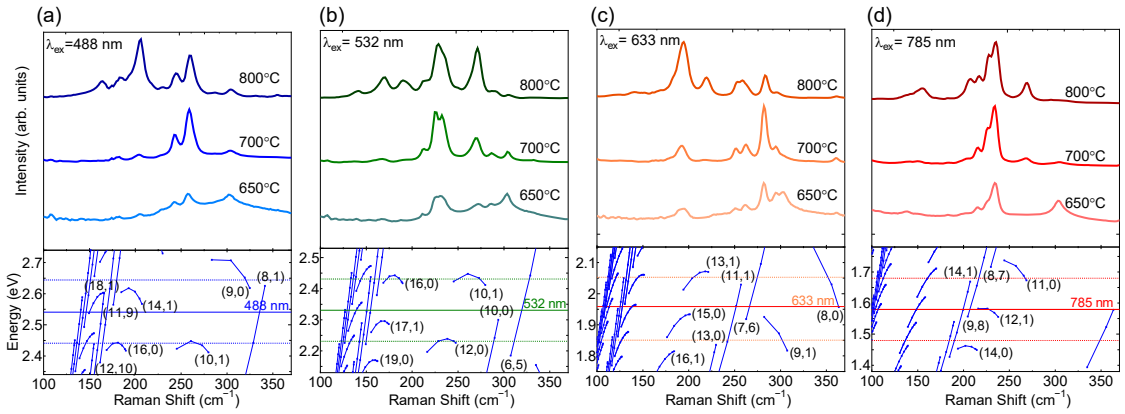

Figure 3. Raman spectra of SWCNTs grown at 800°C, 700°C, and 650°C with water vapor pretreatment. The excitation wavelengths are (a) 488 nm, (b) 532 nm, (c) 633 nm, and (d) 785 nm. The bottom panels represent the Kataura plot [44] of the corresponding energy ranges.

3.4. Chirality analysis of SWCNTs grown with water vapor pretreatment

RBM Raman spectra were analyzed to investigate the chirality distribution of SWCNTs by focusing on the effect of water vapor pretreatment at a low growth temperature. Each spectrum was deconvoluted with the Lorentzian components (Figure S5), and chiralities were assigned based on the peak frequencies and resonant energy [46] using the Kataura plot [44]. Figure 4 depicts the chirality map of the SWCNTs grown at 700°C without water and with water vapor pretreatment. The outline width of the hexagon in the chirality map represents the relative intensity of the RBM peaks for each

excitation wavelength. Note that the intensity of the RBM peaks depends not only on the abundance of SWCNTs with a certain chirality but also on the exciton–photon and exciton–phonon interaction matrix of SWCNTs, which depends on chirality, as well as the energy difference between the chirality-dependent interband transitions of the SWCNTs and the excitation laser [47]. Previous studies have calculated the matrix elements for E^{M}_{11}, E^{S}_{11}, and E^{S}_{22} [48]; however, those for E^{S}_{33} and E^{S}_{44}, which have to be considered for analyzing the present chirality distribution, have never been reported. Hence, we only discuss the relative intensity of the RBM peaks. Without performing water vapor pretreatment, the chiralities of the grown SWCNTs are broadly distributed in terms of the diameters and chiral angles (Figure 4a). After water vapor pretreatment, some of the chiralities with large diameters and small chiral angles are no longer detected, and the peak intensities of several chiralities, including (7,5), (8,5), and (9,6), are highly enhanced (Figure 4b). This indicates that the chirality preference to small diameters and near armchair is attained by water vapor pretreatment. Unlike previous studies [34,35], there is no apparent selectivity to metallic or semiconducting SWCNTs.

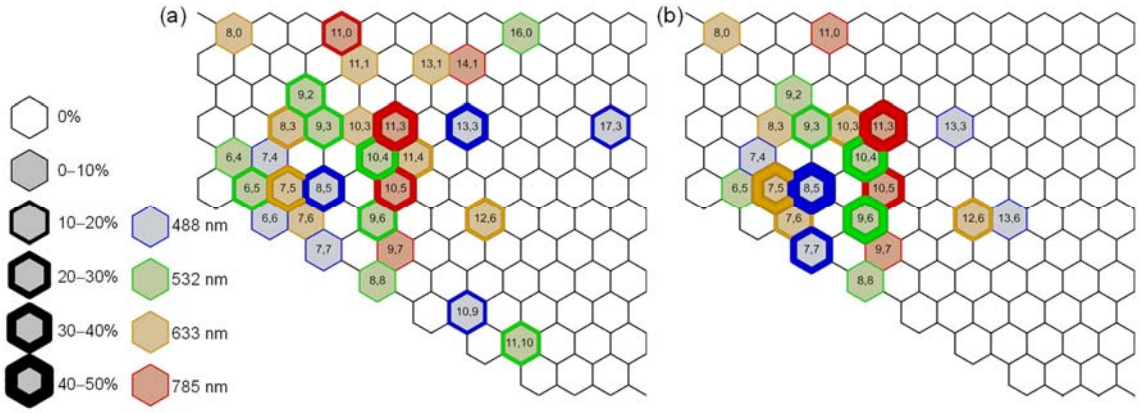

Figure 4. Chirality map of SWCNTs grown at 700°C (a) without and (b) with water vapor pretreatment. The outline width of the hexagon indicates the relative RBM intensity of SWCNTs with the corresponding chirality for each excitation wavelength.

To investigate the chiral angle preferences induced by water vapor pretreatment, the relative RBM intensities were evaluated for chiralities with the same $2n + m$ families and were plotted against the chiral angle, as depicted in Figure 5. For $2n + m = 19$, while the relative intensity of (8,3) decreased because of water vapor pretreatment, the relative intensity of (7,5) increased. For $2n + m = 21$ and 24, the intensities of (8,5) and (9,6) denote the most abundant chiralities after water vapor pretreatment, respectively. These changes in relative RBM intensities clearly indicate near-armchair selectivity, while the amount of armchair SWCNTs with a chiral angle of 30° is not enhanced by water vapor pretreatment.

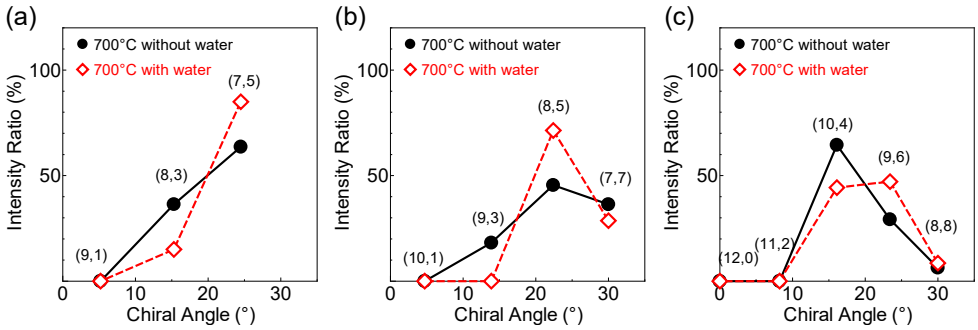

Figure 5. Relative intensity of the RBM peaks of different chiralities with three families where ($2n + m$) is equal to (a) 19, (b) 21, and (c) 24. The SWCNTs are grown at 700°C with and without water vapor pretreatment.

PL spectroscopy [22] was employed to analyze the chirality distribution of SWCNTs. Because dispersed nanotubes with a sufficiently high concentration is required for performing the PL measurements, SWCNTs were grown on six pieces of silicon substrates with ~25-mm square size for each growth condition and dispersed in water with sodium dodecyl sulfate by bath sonication. Figure 6 denotes the PL spectra of SWCNTs grown at 700°C without and with water vapor pretreatment. The PL peaks indicate the existence of various chiralities, including (6,5), (7,6), (7,5), (8,4), (9,4), and (8,6), in the without-water-vapor condition. With water vapor pretreatment, the chirality distribution drastically changed, and peaks of (6,5), (7,5), and (7,6) were obtained as the main components. These chiralities have diameters of 0.8–0.9 nm and chiral angles of approximately 26°–28°. This chirality preference is in good agreement with that observed from the Raman spectra.

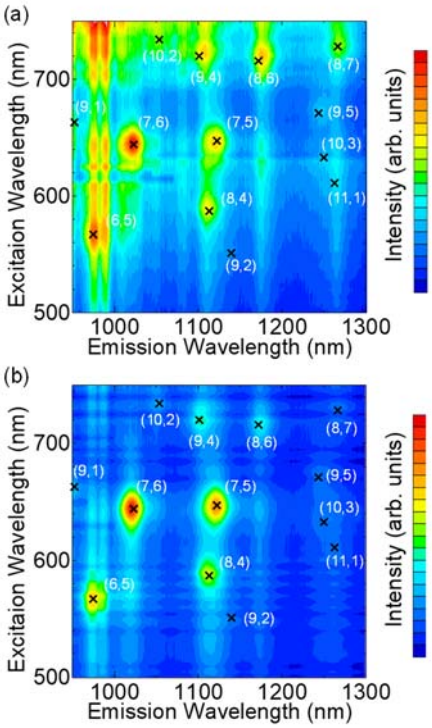

Figure 6. PL spectra of SWCNTs grown at 700°C (a) without and (b) with water vapor pretreatment.

The results indicate that SWCNTs of small diameters and large chiral angles are grown by the water vapor addition. A decrease in tube diameters usually occurs with reduced sizes of catalyst nanoparticles [18,19]; however, in the present study, a drastic change in the catalyst sizes is unlikely because water vapor was introduced after the reduction process, during which the catalyst were formed into nanoparticles. Alternative hypothesis is that water vapor causes a change in the two growth modes: tangential and perpendicular modes, which produce SWCNTs as large as the catalyst diameter and those smaller than the catalyst diameter, respectively [49]. He et al. reported that changing carbon source gas affects the carbon concentration in the catalyst nanoparticles and the interaction between the catalyst and the tube walls, and can switch the two growth modes [26]. Meanwhile, Xu et al. achieved the tuning of the chirality preference from (6,5) to (6,4) by controlling the oxidation degree of the catalyst through pretreatment using a mixture gas of water vapor, hydrogen, and nitrogen and discussed its origin based on the first-principles calculations that shows the oxidation alters the interaction between the catalyst and the carbon structures [39]. Our recent study revealed that catalytic Co nanoparticles are oxidized to Co_3O_4 after heating at 450°C in air and then reduced by ethanol during the SWCNT growth [50]. We consider that oxidation by water vapor and partial reduction by ethanol determine the oxidation state of the catalyst in the present study. Partially oxidized catalyst could cause a change in the catalyst–tube interaction and result in the growth of smaller-diameter SWCNTs through the transition from the tangential mode to the perpendicular mode. Further, in a

recent study, a preference to large chiral angles was energetically modeled with taking into account the configuration entropy with assuming the perpendicular contact between the catalyst and the nanotubes [30]. He et al. also experimentally revealed that the perpendicular mode leads to the near-armchair selectivity while the tangential mode causes no chiral selectivity [26]. It could be possible that the growth modes are critical in the chiral angle selectivity caused by water vapor pretreatment in the present study. Detailed observations of the catalyst–tube interface are beyond the scope of the present work but are worth being conducted in future work for further elucidating the microscopic mechanism.

4. Conclusions

We investigated the effects of water vapor addition on the SWCNT growth using Co/Mo as the catalyst and ethanol as the carbon source. Both the water vapor addition during growth and water vapor pretreatment decreased the diameter of SWCNTs. Water vapor pretreatment also induced a preference to large chiral angles, which indicated the importance of catalyst conditioning for the selective growth of near-armchair SWCNTs. Simple water vapor pretreatment for narrowing chirality distribution can be combined with other CVD systems of SWCNTs and enable the growth of structure-controlled SWCNTs required for electronic and optical applications.

Acknowledgement

Part of this work was financially supported by JSPS KAKENHI Grant Numbers JP15H05760, JP17K06187, JP17K14601, JP18H05329, and JP18K18826. Part of this work was supported by Laser Alliance, the University of Tokyo. We thank Toru Osawa for assistance with PL measurements.

[1] S. Iijima, T. Ichihashi, Single-shell carbon nanotubes of 1-nm diameter, Nature. 363 (1993) 603–605. doi:10.1038/363603a0.

[2] R. Rao, C.L. Pint, A.E. Islam, R.S. Weatherup, S. Hofmann, E.R. Meshot, F. Wu, C. Zhou, N. Dee, P.B. Amama, J. Carpena-Nuñez, W. Shi, D.L. Plata, E.S. Penev, B.I. Yakobson, P.B. Balbuena, C. Bichara, D.N. Futaba, S. Noda, H. Shin, K.S. Kim, B. Simard, F. Mirri, M. Pasquali, F. Fornasiero, E.I. Kauppinen, M. Arnold, B.A. Cola, P. Nikolaev, S. Arepalli, H.-M. Cheng, D.N. Zakharov, E.A. Stach, J. Zhang, F. Wei, M. Terrones, D.B. Geohegan, B. Maruyama, S. Maruyama, Y. Li, W.W. Adams, A.J. Hart, Carbon Nanotubes and Related Nanomaterials: Critical Advances and Challenges for Synthesis toward Mainstream Commercial Applications, ACS Nano. 12 (2018) 11756–11784. doi:10.1021/acsnano.8b06511.

[3] R. Saito, M. Fujita, G. Dresselhaus, M.S. Dresselhaus, Electronic structure of chiral graphene tubules, Appl. Phys. Lett. 60 (1992) 2204–2206. doi:10.1063/1.107080.

[4] H. Liu, D. Nishide, T. Tanaka, H. Kataura, Large-scale single-chirality separation of single-wall

carbon nanotubes by simple gel chromatography, Nat. Commun. 2 (2011) 309. doi:10.1038/ncomms1313.

[5] F. Yang, X. Wang, D. Zhang, J. Yang, Z. Xu, J. Wei, J.-Q. Wang, Z. Xu, F. Peng, X. Li, R. Li, Y. Li, M. Li, X. Bai, F. Ding, Y. Li, Chirality-specific growth of single-walled carbon nanotubes on solid alloy catalysts, Nature. 510 (2014) 522–524. doi:10.1038/nature13434.

[6] S. Zhang, L. Kang, X. Wang, L. Tong, L. Yang, Z. Wang, K. Qi, S. Deng, Q. Li, X. Bai, F. Ding, J. Zhang, Arrays of horizontal carbon nanotubes of controlled chirality grown using designed catalysts, Nature. 543 (2017) 234–238. doi:10.1038/nature21051.

[7] J. Wang, X. Jin, Z. Liu, G. Yu, Q. Ji, H. Wei, J. Zhang, K. Zhang, D. Li, Z. Yuan, J. Li, P. Liu, Y. Wu, Y. Wei, J. Wang, Q. Li, L. Zhang, J. Kong, S. Fan, K. Jiang, Growing highly pure semiconducting carbon nanotubes by electrotwisting the helicity, Nat. Catal. 1 (2018) 326–331. doi:10.1038/s41929-018-0057-x.

[8] Q. Cao, J. Tersoff, D.B. Farmer, Y. Zhu, S. Han, Carbon nanotube transistors scaled to a 40-nanometer footprint, Science (80-.). 356 (2017) 1369–1372. doi:10.1126/science.aan2476.

[9] K. Otsuka, T. Inoue, E. Maeda, R. Kometani, S. Chiashi, S. Maruyama, On-Chip Sorting of Long Semiconducting Carbon Nanotubes for Multiple Transistors along an Identical Array, ACS Nano. 11 (2017) 11497–11504. doi:10.1021/acsnano.7b06282.

[10] X. He, H. Htoon, S.K. Doorn, W.H.P. Pernice, F. Pyatkov, R. Krupke, A. Jeantet, Y. Chassagneux, C. Voisin, Carbon nanotubes as emerging quantum-light sources, Nat. Mater. 17 (2018) 663–670. doi:10.1038/s41563-018-0109-2.

[11] H. Dai, A.G. Rinzler, P. Nikolaev, A. Thess, D.T. Colbert, R.E. Smalley, Single-wall nanotubes produced by metal-catalyzed disproportionation of carbon monoxide, Chem. Phys. Lett. 260 (1996) 471–475. doi:10.1016/0009-2614(96)00862-7.

[12] Y. Shibuta, S. Maruyama, Molecular dynamics simulation of formation process of single-walled carbon nanotubes by CCVD method, Chem. Phys. Lett. 382 (2003) 381–386. doi:10.1016/j.cplett.2003.10.080.

[13] H. Yoshida, S. Takeda, T. Uchiyama, H. Kohno, Y. Homma, Atomic-Scale In-situ Observation of Carbon Nanotube Growth from Solid State Iron Carbide Nanoparticles, Nano Lett. 8 (2008) 2082–2086. doi:10.1021/nl080452q.

[14] P.G. Collins, A. Zettl, H. Bando, A. Thess, R.E. Smalley, Nanotube nanodevice, Science (80-.). 278 (1997) 100. doi:10.1126/science.278.5335.100.

[15] K. Otsuka, S. Yamamoto, T. Inoue, B. Koyano, H. Ukai, R. Yoshikawa, R. Xiang, S. Chiashi, S. Maruyama, Digital Isotope Coding to Trace the Growth Process of Individual Single-Walled Carbon Nanotubes, ACS Nano. 12 (2018) 3994–4001. doi:10.1021/acsnano.8b01630.

[16] Y. Yao, Q. Li, J. Zhang, R. Liu, L. Jiao, Y.T. Zhu, Z. Liu, Temperature-mediated growth of single-walled carbon-nanotube intramolecular junctions., Nat. Mater. 6 (2007) 283–6.

doi:10.1038/nmat1865.

[17] Q. Zhao, Z. Xu, Y. Hu, F. Ding, J. Zhang, Chemical vapor deposition synthesis of near-zigzag single-walled carbon nanotubes with stable tube-catalyst interface, Sci. Adv. 2 (2016) e1501729–e1501729. doi:10.1126/sciadv.1501729.

[18] Y. Li, W. Kim, Y. Zhang, M. Rolandi, D. Wang, H. Dai, Growth of Single-Walled Carbon Nanotubes from Discrete Catalytic Nanoparticles of Various Sizes, J. Phys. Chem. B. 105 (2001) 11424–11431. doi:10.1021/jp012085b.

[19] R. Xiang, E. Einarsson, Y. Murakami, J. Shiomi, S. Chiashi, Z. Tang, S. Maruyama, Diameter Modulation of Vertically Aligned Single-Walled Carbon Nanotubes, ACS Nano. 6 (2012) 7472–7479. doi:10.1021/nn302750x.

[20] S. Maruyama, R. Kojima, Y. Miyauchi, S. Chiashi, M. Kohno, Low-temperature synthesis of high-purity single-walled carbon nanotubes from alcohol, Chem. Phys. Lett. 360 (2002) 229–234. doi:10.1016/S0009-2614(02)00838-2.

[21] N. Pierce, G. Chen, L. P. Rajukumar, N.H. Chou, A.L. Koh, R. Sinclair, S. Maruyama, M. Terrones, A.R. Harutyunyan, Intrinsic Chirality Origination in Carbon Nanotubes, ACS Nano. 11 (2017) 9941–9949. doi:10.1021/acsnano.7b03957.

[22] S.M. Bachilo, M.S. Strano, C. Kittrell, R.H. Hauge, R.E. Smalley, R.B. Weisman, Structure-assigned optical spectra of single-walled carbon nanotubes., Science (80-.). 298 (2002) 2361–6. doi:10.1126/science.1078727.

[23] Y. Miyauchi, S. Chiashi, Y. Murakami, Y. Hayashida, S. Maruyama, Fluorescence spectroscopy of single-walled carbon nanotubes synthesized from alcohol, Chem. Phys. Lett. 387 (2004) 198–203. doi:10.1016/j.cplett.2004.01.116.

[24] H. Wang, L. Wei, F. Ren, Q. Wang, L.D. Pfefferle, G.L. Haller, Y. Chen, Chiral-selective CoSO4/SiO2 catalyst for (9,8) single-walled carbon nanotube growth., ACS Nano. 7 (2013) 614–626. doi:10.1021/nn3047633.

[25] M. Fouquet, B.C. Bayer, S. Esconjauregui, C. Thomsen, S. Hofmann, J. Robertson, Effect of Catalyst Pretreatment on Chirality-Selective Growth of Single-Walled Carbon Nanotubes, J. Phys. Chem. C. 118 (2014) 5773–5781. doi:10.1021/jp4085348.

[26] M. He, Y. Magnin, H. Jiang, H. Amara, E.I. Kauppinen, A. Loiseau, C. Bichara, Growth modes and chiral selectivity of single-walled carbon nanotubes, Nanoscale. 10 (2018) 6744–6750. doi:10.1039/c7nr09539b.

[27] F. Ding, A.R. Harutyunyan, B.I. Yakobson, Dislocation theory of chirality-controlled nanotube growth, Proc. Natl. Acad. Sci. 106 (2009) 2506–2509. doi:10.1073/pnas.0811946106.

[28] R. Rao, D. Liptak, T. Cherukuri, B.I. Yakobson, B. Maruyama, In situ evidence for chirality-dependent growth rates of individual carbon nanotubes, Nat. Mater. 11 (2012) 213–216. doi:10.1038/nmat3231.

[29] V.I. Artyukhov, E.S. Penev, B.I. Yakobson, Why nanotubes grow chiral, Nat. Commun. 5 (2014) 4892. doi:10.1038/ncomms5892.

[30] Y. Magnin, H. Amara, F. Ducastelle, A. Loiseau, C. Bichara, Entropy-driven stability of chiral single-walled carbon nanotubes, Science (80-.). 362 (2018) 212–215. doi:10.1126/science.aat6228.

[31] R.M. Sundaram, K.K.K. Koziol, A.H. Windle, Continuous direct spinning of fibers of single-walled carbon nanotubes with metallic chirality., Adv. Mater. 23 (2011) 5064–8. doi:10.1002/adma.201102754.

[32] K. Hata, D.N. Futaba, K. Mizuno, T. Namai, M. Yumura, S. Iijima, Water-assisted highly efficient synthesis of impurity-free single-walled carbon nanotubes., Science (80-.). 306 (2004) 1362–4. doi:10.1126/science.1104962.

[33] W. Zhou, S. Zhan, L. Ding, J. Liu, General Rules for Selective Growth of Enriched Semiconducting Single Walled Carbon Nanotubes with Water Vapor as in Situ Etchant, J. Am. Chem. Soc. 134 (2012) 14019–14026. doi:10.1021/ja3038992.

[34] A.R. Harutyunyan, G. Chen, T.M. Paronyan, E.M. Pigos, O.A. Kuznetsov, K. Hewaparakrama, S.M. Kim, D. Zakharov, E.A. Stach, G.U. Sumanasekera, Preferential growth of single-walled carbon nanotubes with metallic conductivity., Science (80-.). 326 (2009) 116–20. doi:10.1126/science.1177599.

[35] S. Sakurai, M. Yamada, H. Sakurai, A. Sekiguchi, D.N. Futaba, K. Hata, A phenomenological model for selective growth of semiconducting single-walled carbon nanotubes based on catalyst deactivation, Nanoscale. 8 (2016) 1015–1023. doi:10.1039/C5NR05673J.

[36] B. Hu, H. Ago, N. Yoshihara, M. Tsuji, Effects of Water Vapor on Diameter Distribution of SWNTs Grown over Fe/MgO-Based Catalysts, J. Phys. Chem. C. 114 (2010) 3850–3856. doi:10.1021/jp9112365.

[37] T. Thurakitseree, E. Einarsson, R. Xiang, P. Zhao, S. Aikawa, S. Chiashi, J. Shiomi, S. Maruyama, Diameter Controlled Chemical Vapor Deposition Synthesis of Single-Walled Carbon Nanotubes, J. Nanosci. Nanotechnol. 12 (2012) 370–376. doi:10.1166/jnn.2012.5398.

[38] F. Yang, X. Wang, J. Si, X. Zhao, K. Qi, C. Jin, Z. Zhang, M. Li, D. Zhang, J. Yang, Z. Zhang, Z. Xu, L.-M. Peng, X. Bai, Y. Li, Water-Assisted Preparation of High-Purity Semiconducting (14,4) Carbon Nanotubes, ACS Nano. 11 (2017) 186–193. doi:10.1021/acsnano.6b06890.

[39] B. Xu, T. Kaneko, Y. Shibuta, T. Kato, Preferential synthesis of (6,4) single-walled carbon nanotubes by controlling oxidation degree of Co catalyst, Sci. Rep. 7 (2017) 11149. doi:10.1038/s41598-017-11712-0.

[40] Y. Murakami, Y. Miyauchi, S. Chiashi, S. Maruyama, Direct synthesis of high-quality single-walled carbon nanotubes on silicon and quartz substrates, Chem. Phys. Lett. 377 (2003) 49–54. doi:10.1016/S0009-2614(03)01094-7.

[41] R.A. Jishi, L. Venkataraman, M.S. Dresselhaus, G. Dresselhaus, Phonon modes in carbon nanotubules, Chem. Phys. Lett. 209 (1993) 77–82. doi:10.1016/0009-2614(93)87205-H.

[42] A. Jorio, A. Souza Filho, G. Dresselhaus, M.S. Dresselhaus, A. Swan, M. Ünlü, B. Goldberg, M. Pimenta, J.H. Hafner, C. Lieber, R. Saito, G-band resonant Raman study of 62 isolated single-wall carbon nanotubes, Phys. Rev. B. 65 (2002) 155412. doi:10.1103/PhysRevB.65.155412.

[43] L.G. Cançado, K. Takai, T. Enoki, M. Endo, Y.A. Kim, H. Mizusaki, A. Jorio, L.N. Coelho, R. Magalhães-Paniago, M.A. Pimenta, General equation for the determination of the crystallite size La of nanographite by Raman spectroscopy, Appl. Phys. Lett. 88 (2006) 163106. doi:10.1063/1.2196057.

[44] P.T. Araujo, S.K. Doorn, S. Kilina, S. Tretiak, E. Einarsson, S. Maruyama, H. Chacham, M. Pimenta, A. Jorio, Third and Fourth Optical Transitions in Semiconducting Carbon Nanotubes, Phys. Rev. Lett. 98 (2007) 067401. doi:10.1103/PhysRevLett.98.067401.

[45] B. Hou, C. Wu, T. Inoue, S. Chiashi, R. Xiang, S. Maruyama, Extended alcohol catalytic chemical vapor deposition for efficient growth of single-walled carbon nanotubes thinner than (6,5), Carbon N. Y. 119 (2017) 502–510. doi:10.1016/j.carbon.2017.04.045.

[46] A. Jorio, R. Saito, J.H. Hafner, C. Lieber, M. Hunter, T. McClure, G. Dresselhaus, M.S. Dresselhaus, Structural (n,m) Determination of Isolated Single-Wall Carbon Nanotubes by Resonant Raman Scattering, Phys. Rev. Lett. 86 (2001) 1118–1121. doi:10.1103/PhysRevLett.86.1118.

[47] A. Jorio, C. Fantini, M. Pimenta, R. Capaz, G. Samsonidze, G. Dresselhaus, M.S. Dresselhaus, J. Jiang, N. Kobayashi, A. Grüneis, R. Saito, Resonance Raman spectroscopy (n,m)-dependent effects in small-diameter single-wall carbon nanotubes, Phys. Rev. B. 71 (2005) 075401. doi:10.1103/PhysRevB.71.075401.

[48] K. Sato, R. Saito, A.R.T. Nugraha, S. Maruyama, Excitonic effects on radial breathing mode intensity of single wall carbon nanotubes, Chem. Phys. Lett. 497 (2010) 94–98. doi:10.1016/j.cplett.2010.07.099.

[49] M.-F.C. Fiawoo, A.-M. Bonnot, H. Amara, C. Bichara, J. Thibault-Pénisson, A. Loiseau, Evidence of Correlation between Catalyst Particles and the Single-Wall Carbon Nanotube Diameter: A First Step towards Chirality Control, Phys. Rev. Lett. 108 (2012) 195503. doi:10.1103/PhysRevLett.108.195503.

[50] Y. Qian, H. An, T. Inoue, S. Chiashi, R. Xiang, S. Maruyama, A Comparison Between Reduced and Intentionally Oxidized Metal Catalysts for Growth of Single-Walled Carbon Nanotubes, Phys. Status Solidi. 1800187 (2018) 1800187. doi:10.1002/pssb.201800187.

Supporting Information

Growth of single-walled carbon nanotubes by alcohol chemical vapor deposition with water vapor pretreatment: Narrowing the diameter and chiral angle distributions

Hiroki Takezaki [a], Taiki Inoue [a], Rong Xiang [a], Shohei Chiashi [a], and Shigeo Maruyama [a,b,*]

[a] Department of Mechanical Engineering, The University of Tokyo, 7-3-1 Hongo, Bunkyo-ku, Tokyo 113-8656, Japan

[b] Energy NanoEngineering Laboratory, National Institute of Advanced Industrial Science and Technology (AIST), 1-2-1 Namiki, Tsukuba 305-8564, Japan

[*] Corresponding author.

E-mail address: maruyama@photon.t.u-tokyo.ac.jp (S. Maruyama)

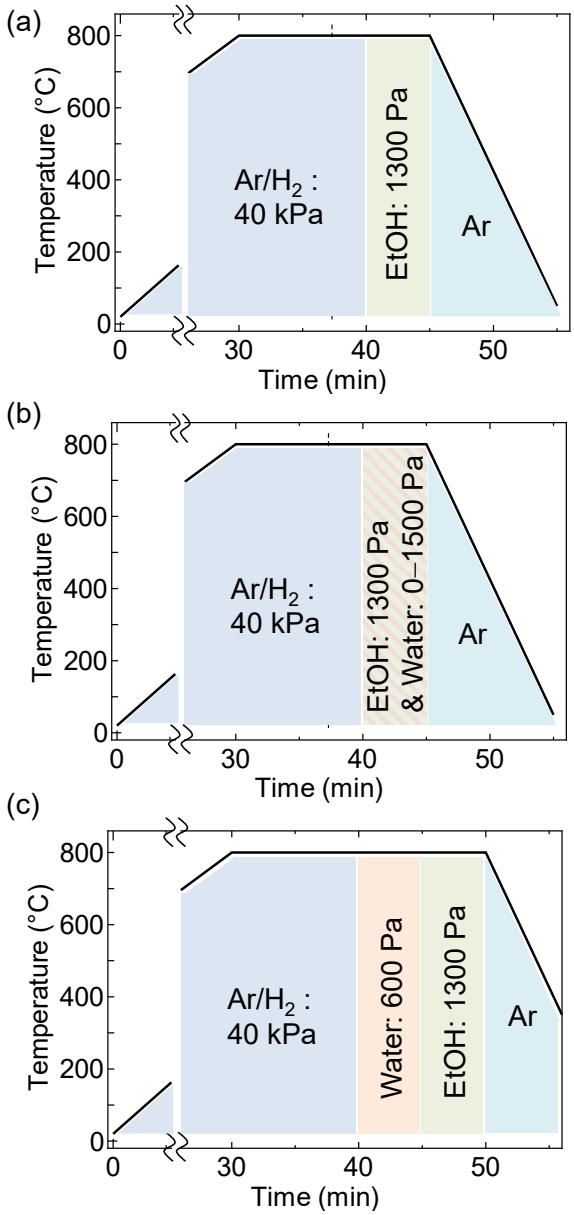

Figure S1. Temperature and gas flow profiles for CVD growth of SWCNTs: (a) without water vapor, (b) with water vapor during growth, and (c) with water vapor before growth (water vapor pretreatment).

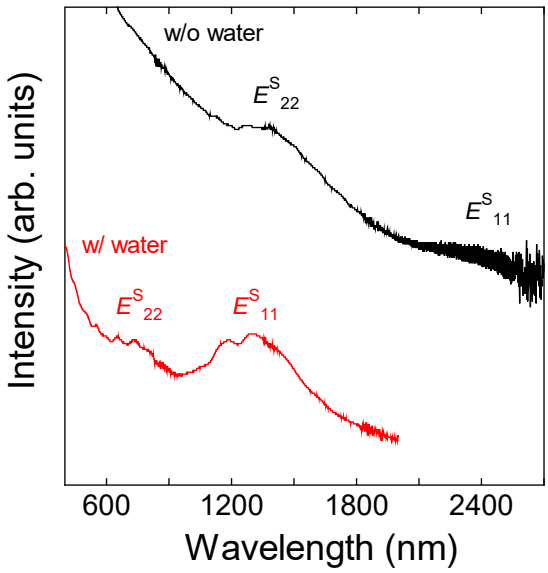

Figure S2. Optical absorption spectra of SWCNTs grown at 800°C without water (black) and with water vapor pretreatment (red).

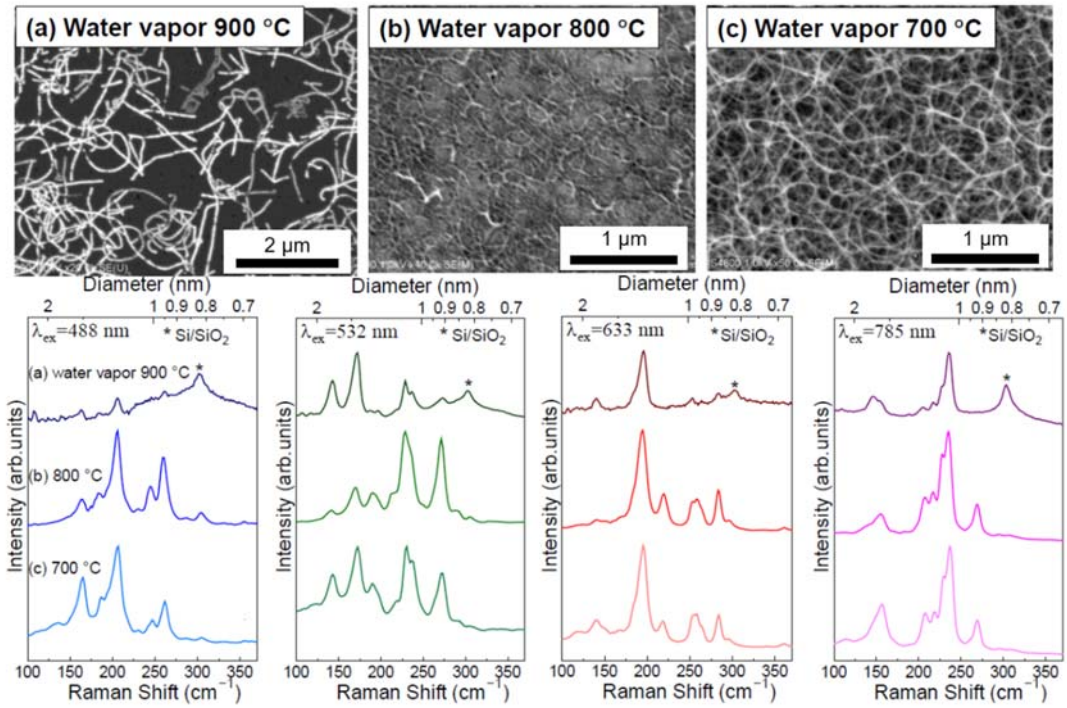

Figure S3. Effects of water vapor pretreatment temperature on SWCNT growth: (a) 900°C, (b) 800°C, and (c) 700°C. Water vapor pressure is 600 Pa. Growth temperature is 800°C. **Top**: SEM images. **Bottom**: Raman RBM spectra for different excitation wavelengths.

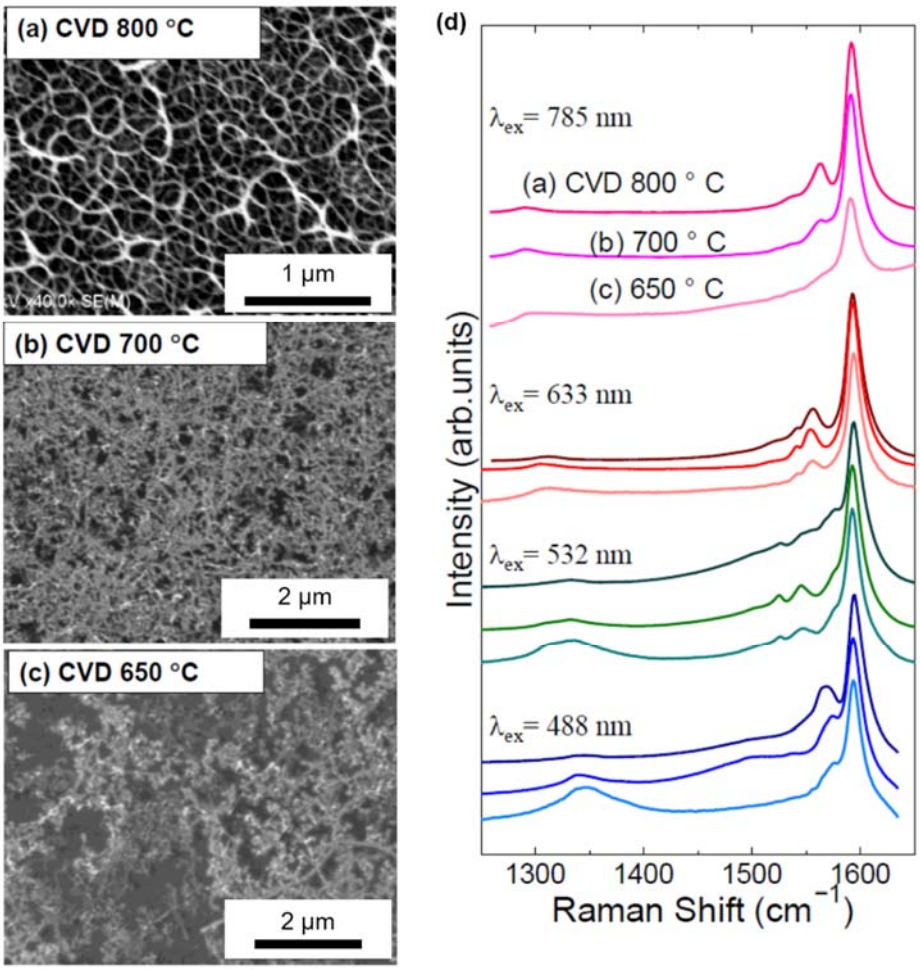

Figure S4. (a–c) SEM images and (d) G-band Raman spectra of SWCNTs grown at (a) 800°C, (b) 700°C, and (c) 650°C with water vapor pretreatment.

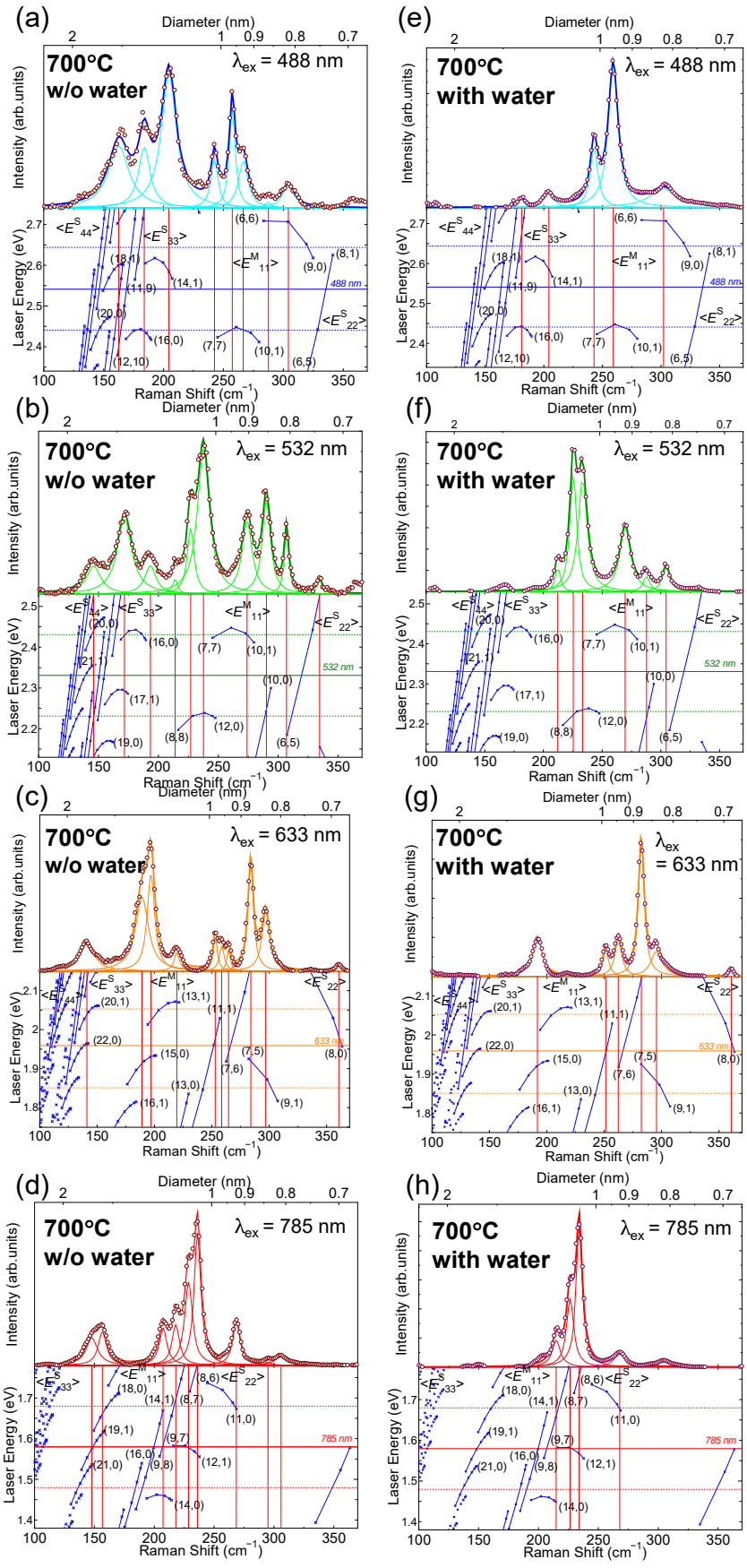
(a)
700°C
w/o water
λex = 488 nm
(e)
700°C
with water
λex = 488 nm
(b)
700°C
w/o water
λex = 532 nm
(f)
700°C
with water
λex = 532 nm
(c)
700°C
w/o water
λex = 633 nm
(g)
700°C
with water
λex = 633 nm
(d)
700°C
w/o water
λex = 785 nm
(h)
700°C
with water
λex = 785 nm
Diameter (nm)
Intensity (arb.units)
Laser Energy (eV)
Raman Shift (cm−1)
488 nm
532 nm
633 nm
785 nm

Figure S5. Peak deconvolution of RBM spectra of SWCNTs grown at 700°C (a–d) without water vapor and (e–f) with water vapor pretreatment. Excitation wavelengths are (a,e) 488 nm, (b,f) 532 nm, (c,g) 633 nm, and (d,h) 785 nm.